Generation mechanism of quasidecadal variability of upper ocean heat content in the equatorial Pacific Ocean

doi: 10.1029/2006JC003755

Generation mechanism of quasidecadal variability of upper ocean heat content in the equatorial Pacific Ocean

Takuya Hasegawa,[1,2] Tamaki Yasuda,[1] and Kimio Hanawa[3]

Received 13 June 2006; revised 23 May 2007; accepted 11 June 2007; published 21 August 2007.

[1] We investigate the relationship between oceanic and atmospheric anomaly fields in the tropical Pacific on the quasidecadal (QD; 10 to 18 years) scale is explored. It is suggested that the anomalous wind stress curl in the tropical South Pacific can generate the equatorial upper ocean heat content (OHC) anomalies on the QD scale via the Sverdrup transport resembling that of the recharge-discharge oscillator model for the dynamics of El Niño-Southern Oscillation (ENSO). The results also show that the wind stress curl anomalies in the tropical South Pacific are accompanied by ENSO-like, QD-scale anomaly patterns of the sea level pressure and sea surface temperature. Furthermore, the results indicate that the equatorial QD-scale OHC anomalies can also be generated by the ENSO-like propagations of the OHC anomalies in the tropical North and South Pacific. This study presents a systematic linkage between the ENSO-like, QD-scale OHC propagation in the tropical North and South Pacific, the Sverdrup transport variation in the tropical South Pacific, and the ENSO-like, QD-scale SST and SLP anomalies in the tropical Pacific.

Citation: Hasegawa, T., T. Yasuda, and K. Hanawa (2007), Generation mechanism of quasidecadal variability of upper ocean heat content in the equatorial Pacific Ocean, *J. Geophys. Res.*, *112*, C08012, doi:10.1029/2006JC003755.

1. Introduction

[2] Previous studies have investigated long-term variations of the sea surface temperature (SST) and atmospheric anomalies over the Pacific or the whole Earth [e.g., *Nitta and Yamada*, 1989; *Trenberth*, 1990; *Tanimoto et al.*, 1993, 1997; *Mann and Park*, 1996; *Mantua et al.*, 1997; *Minobe*, 1997, 1999; *Zhang et al.*, 1997; *White and Cayan*, 1998; *Tourre et al.*, 2001; *Yasunaka and Hanawa*, 2002, 2003, 2005; *Deser et al.*, 1999]. It was pointed out that the long-term variations of the SST and atmospheric anomaly fields also display El Niño-Southern Oscillation (ENSO)-like spatial patterns. *Mantua et al.* [1997] named an interdecadal-scale (about 20 years in period) variation found in the SST and atmospheric anomaly fields in the Pacific as the "Pacific Decadal Oscillation (PDO)." The PDO displays an ENSO-like spatial pattern but has a strong climate signal in the midlatitudes of the North Pacific in contrast to ENSO [*Mantua et al.*, 1997]. *Minobe* [1999] showed that the dominant timescale of the PDO are also found on the pentadecadal (about 50 years in period) scale as well as the interdecadal scale.

[3] *Tourre et al.* [2001] showed that spectrum peaks of the Pacific SST and SLP anomalies can also be found on a quasidecadal (QD) scale. The dominant timescale of the QD scale variability is about 11 years in period, which is shorter than that of the PDO. In addition, they showed that the QD signal also displays ENSO-like spatial patterns with large signals in the tropical Pacific, in contrast to the PDO. They also showed that the QD-scale and interdecadal-scale variations have distinct spatial evolutions, and they suggested that the two variations invoke different physical processes in order to maintain their signals; the former requires Rossby wave propagations and the latter does advection by the mean gyre circulation [*White and Cayan*, 1998].

[4] Recently, observed subsurface ocean thermal data have been available and several authors have analyzed an upper ocean heat content (OHC) anomaly field on the QD scale in the tropical Pacific. Among them, *Luo and Yamagata* [2001] suggested that the QD-scale OHC anomalies in the tropical South Pacific are produced by local wind stress curl anomalies. OHC anomalies then move northwestward toward the equator. After reaching the equator, they propagate eastward along the equator. They also noted that, unlike the South Pacific, the North Pacific does not contribute to the generation of the equatorial thermal anomalies.

[5] On the other hand, *White et al.* [2003] showed that the westward propagating, QD-scale OHC anomalies, both in the tropical South and North Pacific, can affect the thermal field in the equatorial Pacific. They showed that westward propagating OHC anomalies along the off-equatorial latitudinal belt between 10°N–20°N get reflected at the western boundary, and then move eastward along the equator toward the central/eastern equatorial Pacific. Such counterclockwise propagation characteristics are similar to those found on the ENSO scale [e.g., *Kessler*, 1990; *Zhang and Levitus*, 1996; *Hasegawa and Hanawa*, 2003a, 2007; *White et al.*,

[1] Meteorological Research Institute, Japan Meteorological Agency, Tsukuba, Japan.
[2] Now at Japan Agency for Marine-Earth Science and Technology, Yokosuka, Japan.
[3] Department of Geophysics, Tohoku University, Sendai, Japan.

0148-0227/07/2006JC003755$09.00

2003]. In addition to this westward propagation in the off-equatorial tropical North Pacific, they showed that westward OHC propagations also appear in the tropical South Pacific in the QD scale. Such QD-scale OHC propagations were also shown by *Hasegawa and Hanawa* [2003b]. Furthermore, *White et al.* [2003] suggested that the off-equatorial, westward propagating, QD-scale OHC anomalies in both the South and North Pacific are generated via anomalous Ekman pumping by the local wind stress curl anomalies to the west of the International Date Line. The QD-scale propagation characteristics were also seen from numerical simulations using coupled models [e.g., *Knutson and Manabe*, 1998; *Yukimoto et al.*, 2000; *Tourre et al.*, 2005].

[6] In order to explain the dynamics of ENSO, several hypotheses have been proposed. Among them, the "delayed action oscillator model" [*Suarez and Schopf*, 1998] emphasize that an equatorial Rossby wave with an OHC anomaly, with a sign opposite to the ongoing ENSO phase, propagates westward in the latitudinal belt from 3°N to 7°N, and then moves toward the equator along the western boundary to form an equatorial Kelvin wave. This Kelvin wave breaks down the air-sea coupled positive feedback of the ongoing ENSO phase and causes an opposite phase of the ENSO when it reaches the central to eastern equatorial Pacific. Although the eastward propagating OHC anomaly along the equator found on the QD scale is similar to the eastward propagating nature of the delayed action oscillator model, the latitudes of the westward propagating QD-scale OHC anomalies are much higher than those expected by this model. On the other hand, the "western Pacific oscillator model" of *Weisberg and Wang* [1997] emphasizes off-equatorial Rossby waves along the latitudinal belt between 10°N and 20°N west of the International Date Line, in addition to the eastward propagations of the OHC anomalies along the equator. Therefore it can be said that the off-equatorial, westward OHC anomalies found on the QD scale have similar propagation characteristic to that of the western Pacific oscillator model as compared to the delayed action oscillator model.

[7] Another model for the ENSO dynamics called the "recharge-discharge oscillator model" was also proposed by *Jin* [1996, 1997a, 1997b]. This model emphasizes the equatorial OHC anomalies caused by the Sverdrup transport anomalies, associated with the off-equatorial wind stress curl anomalies, as follows. During warm (cold) ENSO events, cyclonic (anticyclonic) wind stress anomaly fields occur in the off-equatorial North and South Pacific, which leads poleward (equatorward) Sverdrup transport from (into) the equatorial region. Eventually, the OHC anomalies in the entire equatorial Pacific are decreasing (increasing) in their magnitudes during this period. When the OHC in the equatorial Pacific is well discharged (recharged) by the poleward (equatorward) Sverdrup transport, the equatorial upwelling becomes strong (weak) and the warm (cold) ENSO event tends to terminate. *Hasegawa and Hanawa* [2003b] showed the a phase relationship between the equatorial OHC and SST anomalies on the QD scale, which is similar to that expected by the recharge-discharge oscillator model, in addition to the ENSO-like propagating OHC anomalies in the tropical North and South Pacific on the QD scale. According to their study, the QD-scale OHC anomalies in the entire equatorial Pacific are decreasing (increasing) in magnitude during the period when the QD-scale SST anomalies in the Niño-3 region are positive (negative). This behavior is very similar to that found on the ENSO scale [e.g., *Meinen and McPhaden*, 2000; *Kessler*, 2002; *Hasegawa and Hanawa*, 2003a; *Hasegawa et al.*, 2006]. This finding is supported by the results of numerical model experiments performed by *Wang et al.* [2003], who indicated that an increase (decrease) of the OHC anomalies in the equator is closely associated with the equatorward (poleward) Sverdrup transport anomalies accompanied by wind stress anomalies in the tropical Pacific on the QD scale. Furthermore, coupled general circulation model experiments also showed a behavior similar to that proposed by the recharge-discharge oscillator model and suggested an important role of the tropical South Pacific in the generation of the equatorial OHC anomalies [*Luo et al.*, 2003].

[8] It is not yet fully understood how the recharge-discharge oscillator model-like behavior on the QD scale relates to the ENSO-like, QD-scale propagation of OHC anomalies in the tropical Pacific. At present, it is also unclear how this behavior associates with the ENSO-like, QD-scale SST and atmospheric anomaly variations in the tropical Pacific. In the present study, we focus the OHC variation on the QD scale in the tropical Pacific, and the purpose of this study is to explore the relationship among the recharge-discharge oscillator model-like behavior of the equatorial OHC anomalies, SST and atmospheric anomaly fields in the tropical Pacific, and also the ENSO-like OHC propagations in the off-equatorial North and South Pacific with special reference to the QD scale. The remainder of this paper is organized as follows. Section 2 describes the data and methodology used in the present study. In section 3 we show the results. Section 4 provides summary and discussion.

2. Data and Methodology

[9] In the present study the global subsurface ocean temperature data provided by the Scripps Institution of Oceanography [*White*, 1995] is used to calculate the OHC anomaly field. The data set is produced by an optimum interpolation method for temperature profiles mostly measured by XBT (expendable bathythermograph), MBT (mechanical bathythermograph), CTD (conductivity-temperature-depth recorder), and TOGA (Tropical Ocean and Global Atmosphere)-TAO (Tropical Atmosphere Ocean) array. The data are given at 11 standard levels of depth from the sea surface down to 400 m (0 m, 20 m, 40 m, 60 m, 80 m, 120 m, 160 m, 200 m, 240 m, 300 m, and 400 m). In this study, vertically averaged temperature from the sea surface to a depth of 300 m is used as a proxy for the OHC. The reason for choosing a depth of 300 m is that it is near the maximum depth to which surface oceanic mixing extends [*Ladd and Thompson*, 2000], and besides the number of observations reaching deeper than 300 m were very few before the late 1970s. The analysis region is the Pacific Ocean (30°S–60°N) with a horizontal resolution of 2° (latitude) × 5° (longitude). In order to remove the noise and smooth the data spatially, we adopt a nine-point median filter (five points in the zonal direction and three points in the meridional direction and time direction) and a Gaussian filter having an *e*-folding scale of 2° in the zonal and meridional directions. In addition, we use reanalysis data

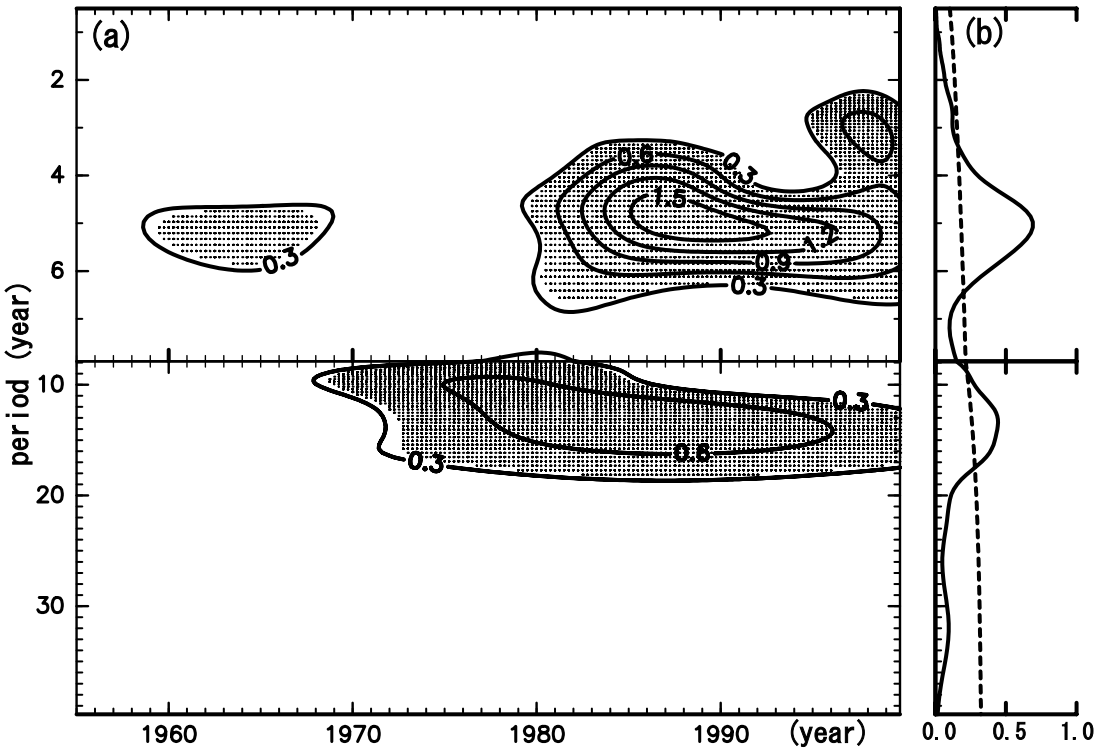

Figure 1. (a) Time period diagram of local power of the 5-month running mean *OHC-EP* (OHC anomalies spatially averaged in the entire equatorial Pacific; see text). The contour interval is $0.3°C^2$. The values exceeding a 10% significance level (within a confidence limit of 90%) for white noise are marked by black dots. (b) Global wavelet spectrum of *OHC-EP* during each period (solid line). The horizontal axis of Figure 1b indicates the magnitude of global wavelet spectrum. A significance level of 10% for white noise is shown by broken line. Note that the scale of the vertical axis for periods shorter than 8 years is exaggerated.

sets of the sea level pressure (SLP) and wind stress prepared by the National Centers for Environmental Prediction/National Center for Atmospheric Research (NCEP/NCAR) [*Kalnay et al.*, 1996]. We also use the SST data set of *Smith and Reynolds* [2003]. The PDO index is provided by the Joint Institute for the Study of the Atmosphere and Ocean (JISAO) of the University of Washington. The PDO index is defined as the first principal component of the North Pacific monthly SST anomalies (poleward of 20°N) [*Mantua et al.*, 1997].

[10] The analysis period is from January 1955 to December 1999 for all the variables. Monthly climatologies at each grid point are made by averaging the variables for individual calendar months for the 45 years, and then the monthly anomalies are calculated by subtracting the monthly climatologies from the individual values. The monthly anomalies are then averaged for each season. Here boreal winter is regarded as three consecutive months from January through March for the SST and OHC anomalies (December through February for atmospheric anomalies), and so on for other seasons.

3. Results

3.1. Dominant Timescales of the OHC Anomalies in the Equatorial Pacific

[11] First we investigate whether the OHC anomalies in the entire equatorial Pacific (*OHC-EP*: OHC anomalies spatially averaged over 6°S–6°N, 130°E–80°W, where "*EP*" stands for the equatorial Pacific), which is an indicator of the recharge-discharge oscillator model, have the QD-scale signal or not. Figure 1 displays the results of a wavelet analysis using the Morlet wavelet (for details of the wavelet analysis, see *Torrence and Compo* [1998]) for the *OHC-EP*. Dominant variations which are manifestation of ENSO having timescale ranging from 3 to 6 years in period are found. In addition, a peak of global wavelet spectrum can also be seen on the QD scale with periods from 10 to 18 years (Figure 1b). The latter timescale variation is present after the early 1970s (Figure 1a). Figure 1 also displays a multidecadal signal with a period of around 30 years. However, the power of the multidecadal scale is very weak. It might be due to that the data length of the OHC data may not be long enough for treatment of the multidecadal scale. For the investigation of the multidecadal OHC anomalies, the analysis of outputs from fully coupled model experiments driven over 100 years is one of the useful approaches. In the present study, we focus on the QD-scale variability of the OHC and other associated variables over the tropical Pacific as described above.

[12] The QD scale found in Figure 1 is consistent with that of previous studies on the equatorial OHC anomalies [e.g., *Luo and Yamagata*, 2001; *Hasegawa and Hanawa*, 2003b, 2006]. However, this timescale is somewhat different from the well-known QD scale, which has a period of 9 to 12 years [*Allan*, 2000; *Tourre et al.*, 2001; *White and*

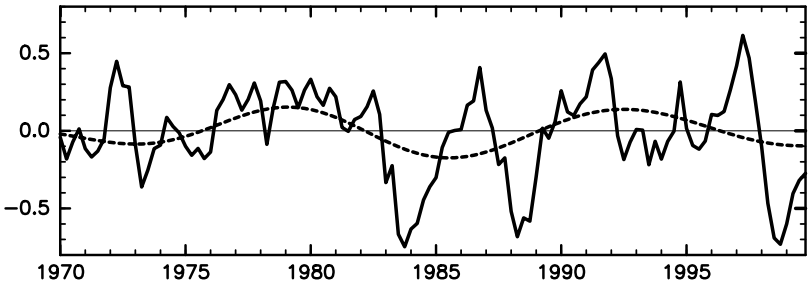

Figure 2. Time series of the unfiltered *OHC-EP* anomalies (°C) (solid line) and the QD-scale *OHC-EP* anomalies (°C) (dashed line).

Cayan, 2000]. This difference may be due to the fact that the well-known QD scale was pointed out by analyzing the SST and SLP anomalies over the whole Pacific basin or a wider area and for much longer period (over 90 years) than that of the present study. The dominant band on the QD scale in Figure 1b covers the most dominant band of the well-known QD scale. Therefore the present results support previous studies based on the analysis of the equatorial OHC anomalies. We refer to the timescale with periods from 10 to 18 years as the "QD scale" hereafter in this paper, and we will deal with the data after the year 1970 for all the variables, when the QD-scale variations are relatively dominant. On the basis of these results, all the variables are band-pass filtered by using the same wavelet filter as that used in Figure 1 with a window from 10 to 18 years in period for analyzing QD-scale variations. Figure 2 shows the time series of the QD-scale *OHC-EP* and unfiltered *OHC-EP*. We can see that the peaks of the positive (negative) QD anomalies are found around the year 1979 and 1992 (1973 and 1986). In the next subsection, we will investigate the relationship between the *OHC-EP* and the atmospheric anomaly fields.

3.2. Relationship Between the Equatorial OHC Anomalies and the Sverdrup Transport in the Tropical Pacific

[13] Figure 3 shows a spatial distribution of correlation coefficients between time derivative of the *OHC-EP* and the Ekman pumping velocity (EPV; positive values denote downwelling, and negative, upwelling) anomalies, which is calculated by use of the NCEP/NCAR wind stress data by assuming a constant seawater density of 1028 kg/m^3, at each grid point on the QD scale. It is seen that correlation coefficients have large positive values greater than 0.50 in the region centered on the zonal belt of 14°S–4°S from 180° to 120°W in the tropical South Pacific. This result means that the decrease (increase) of the QD-scale *OHC-EP* in their magnitudes is associated with the negative (positive) EPV anomalies in the tropical South Pacific.

[14] In order to clarify the relationship between the EPV in the tropical South Pacific (14°S–4°S, 180°–120°W) and the *OHC-EP*, we prepare the time series of the EPV anomalies averaged in the tropical South Pacific and the *OHC-EP* (Figure 4). In Figure 4, we can see that overall the *OHC-EP* are decreasing (increasing) in their magnitudes, when the EPV anomalies in the tropical South Pacific take negative (positive) values. Indeed, the correlation coefficient between the temporal changes of the QD-scale *OHC-EP* and the EPV in the tropical South Pacific is 0.92 (Table 1). This suggests that the negative (positive) EPV anomalies in the tropical South Pacific generate the poleward (equatorward) Sverdrup transport anomalies there, thus leading to a decrease (increase) in magnitudes of the *OHC-EP* in the tropical South Pacific. To investigate the relationship between the *OHC-EP*, the Sverdrup transport, and the EPV anomalies in this region, we plot the QD-scale

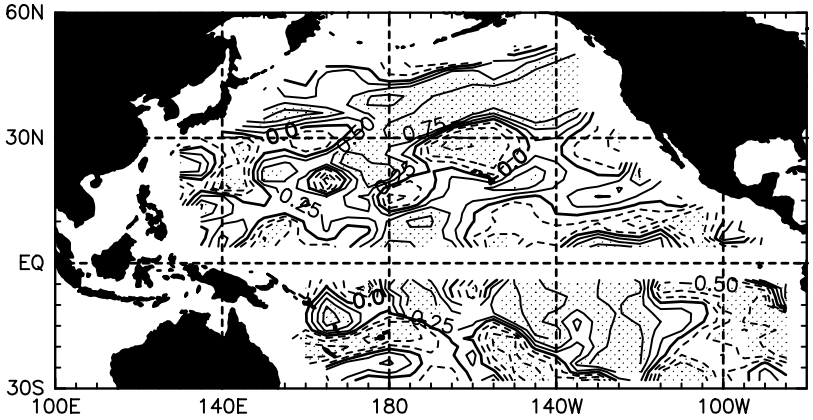

Figure 3. Spatial distribution of correlation coefficients between the time derivative of the QD-scale *OHC-EP* and the QD-scale EPV anomalies at each grid point. Contour interval is 0.25 and the dashed line indicates negative values. Dotted region indicates values exceeding a significance level of 10% (within a confidence limit of 90%) for the Student *t*-test.

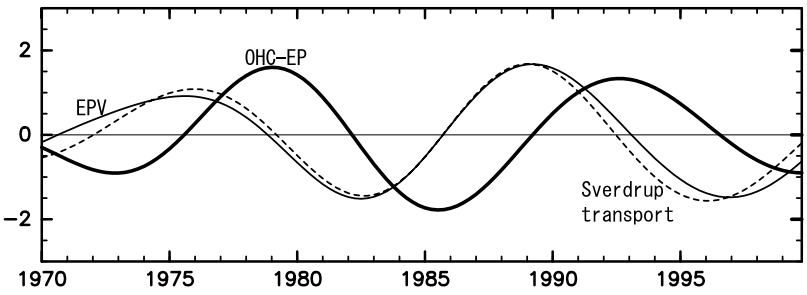

Figure 4. Time series of the *OHC-EP* (thick solid line), the EPV anomalies spatially averaged over the tropical South Pacific (14°S–4°S, 180°–120°W: thin solid line) and the Sverdrup transport anomaly zonally integrated from the eastern boundary at [6°S, 90°W] to the western boundary [6°S, 160°E] in the tropical South Pacific calculated from the NCEP/NCAR wind stress data (thin dashed line; positive and negative values denote equatorward and poleward transport, respectively) on the QD scale. Values are normalized by their standard deviations.

Sverdrup transport anomalies zonally integrated from the eastern boundary at [6°S, 90°W] to the western boundary at [6°S, 140°E] in the South Pacific in Figure 4. We can see that the poleward (equatorward) Sverdrup transports anomalies from (into) the equatorial Pacific appear, when the negative (positive) EPV anomalies appear in the tropical South Pacific and the *OHC-EP* are decreasing (increasing) in their magnitudes. A correlation coefficient between the EPV and Sverdrup transports along 6°S is 0.93 and a correlation coefficient between the time derivative of the QD-scale *OHC-EP* and the Sverdrup transports along 6°S is 0.96 (Table 1).

[15] In order to clarify the effect of the Sverdrup transports on the generation of the *OHC-EP*, we simply estimate the temporal changes of the *OHC-EP* due to variations of the Sverdrup transport in the South Pacific (Figure 5a). For this, we assume that the upper ocean (sea surface to a depth of 300 m) consists of two layers including the first layer having a temperature of 25°C and the second layer at 15°C, on the basis of observational evidence [*Colin et al.*, 1971]. It is also assumed that 50% of the total amount of the Sverdrup transport affects the volume changes of the first layer, although it is unclear how much the Sverdrup transport affects the first layer volume changes exactly at present. The volume changes of the second layer are set to counterbalance the increase and decrease of the volume of the first layer. Finally, we calculate temporal changes of the *OHC-EP* due to the temporal changes in the volumes of the upper ocean layers by the Sverdrup transport as follows:

$$OHCc = (T1 - T2) \times (Vc/V),$$

where, *OHCc* is the temporal change of the *OHC-EP* due to the Sverdrup transport variation in the South Pacific (°C/season), $T1$ and $T2$ are the temperature of the first and second layers respectively, *Vc* is the temporal changes in the volume of the first layer due to the Sverdrup transport variation, and V is the volume of the *OHC-EP*. It can seen from Figure 5a that the temporal changes of the OHC anomalies due to the Sverdrup transport in the South Pacific are in phase with the temporal changes of the observed *OHC-EP*, having a correlation coefficient of 0.96. It is also shown that the Sverdrup transport can account for a large part of the changes in the *OHC-EP*, particularly after the year 1985. The standard deviations of the temporal changes of the observed *OHC-EP* and the temporal changes of the OHC anomalies due to the Sverdrup transport are 0.011°C/season and 0.008°C/season, respectively. That is, the Sverdrup transport can account for roughly 73% of the *OHC-EP* changes during the analysis period under the above assumption. Therefore, even though it is not perfectly understood how much the Sverdrup transport actually affects the changes in the volume of the upper layer, this result suggests the Sverdrup transport in the tropical South Pacific has the potential to generate the *OHC-EP* variations on the QD scale to some extent.

[16] Figure 3 shows that the correlation coefficients between the *OHC-EP* and the EPV has no large positive values in the wide area of the tropical North Pacific in contrast to the tropical South Pacific. This suggests that the Sverdrup transport in the North Pacific does not have a strong influence on the *OHC-EP*. Indeed we can see from Figure 5b that the temporal changes of the *OHC-EP* due to the Sverdrup transport in the North Pacific is not in phase with the temporal changes of the observed *OHC-EP*. The correlation coefficient between the two variables is about 0.05. Thus it should be concluded that the Sverdrup transport cannot explain the *OHC-EP* changes in the North Pacific. Therefore these results indicate that a decrease (increase) in the QD-scale *OHC-EP* link to the poleward (equatorward) Sverdrup transport anomalies in the tropical South Pacific in association with the negative (positive) EPV anomalies that are present there. The relationship among them is similar to that expected from the recharge-discharge oscillator model for the ENSO dynamics. However, it should be noted that there is a difference between the

Table 1. Correlation Coefficients Between Time Derivative of the *OHC-EP*, the EPV Anomalies Spatially Averaged Over the Tropical South Pacific (14°S–4°S, 180°–120°W), and the Sverdrup Transport at [6°S, 160°E] on the QD Scale[a]

	EPV	Sverdrup Transport
Time derivative of *OHC-EP*	0.92	0.96
EPV		0.93

[a]Values greater than 0.72 or less than −0.72 exceed a significance level of 5% (within a confidence limit of 95%) for the Student *t*-test.

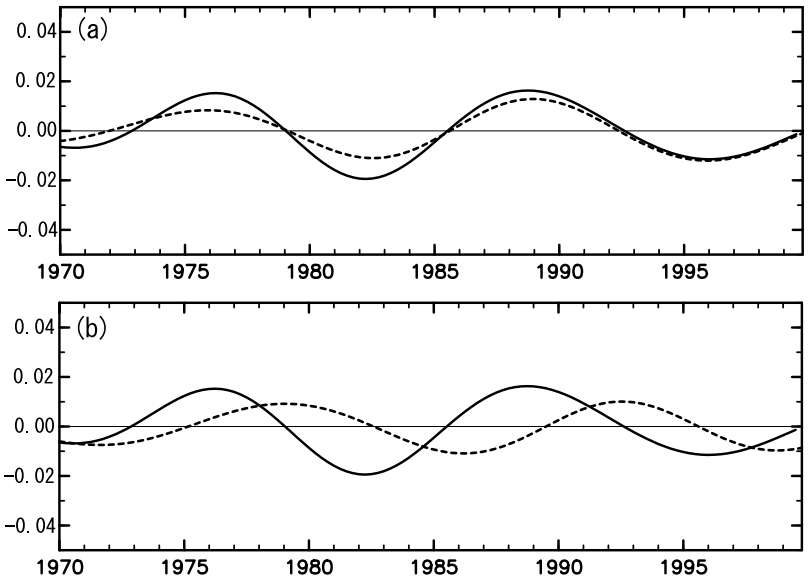

Figure 5. (a) Time series of the temporal changes of the observed *OHC-EP* (thick solid line; °C/season) and the temporal changes of the *OHC-EP* due to the Sverdrup transport anomaly zonally integrated from the eastern boundary of the tropical South Pacific at [6°S, 90°W] to the western boundary of the tropical South Pacific at [6°S, 160°E] (thin solid line; °C/season) on the QD scale. (b) Same as Figure 5a but temporal changes of the observed *OHC-EP* (thick solid line; °C/season) and the temporal changes of the *OHC-EP* due to the Sverdrup transport anomaly zonally integrated from the eastern boundary of the tropical North Pacific at [6°N, 90°W] to the western boundary of the tropical North Pacific at [6°N, 140°E] (thin solid line; °C/season) on the QD scale.

QD and the ENSO scales. That is, the recharge-discharge oscillator model-like behavior is not observed in the North Pacific on the QD scale, in contrast to the ENSO scale [e.g., *Meinen and McPhaden*, 2000; *Hasegawa and Hanawa*, 2003a].

[17] Figure 6a shows that the spatial distribution of correlation coefficients between the EPV anomalies averaged over the tropical South Pacific and the zonal wind stress anomalies. As can be seen from Figure 6a, the positive (negative) EPV anomalies in the tropical South Pacific are associated with a meridional shear of zonal wind stress due to the easterly (westerly) zonal wind stress anomalies centered in the area south of the equator (10°S–4°S, 180°–120°W), and the westerly (easterly) wind stress anomalies south of 14°S. Figure 6b is a snapshot for the EPV and wind stress anomalies in winter of the year 1983, when the EPV anomalies in the tropical South Pacific take its negative peak (see Figure 4). In line with the result of correlation analysis, the negative EPV anomalies in the tropical South Pacific accompany a cyclonic pattern with the westerly wind stress anomalies (10°S–4°S, 180°–120°W) and the easterly wind stress anomalies (south of 14°S). Although not shown here, periods for other negative EPV anomalies (e.g., the year 1997) shows similar wind stress patterns, and periods for positive EPV anomalies (e.g., the year 1976 and the year 1989) shows similar wind stress pattern with opposite sign. It is worth noting that the location of the wind stress variations described here is near the position of the southeast trade winds and South Pacific Convergence Zone (SPCZ), so that the wind stress variations, which can affect the *OHC-EP* via Sverdrup transport, may be associated with changes in the intensity of the southeast trade winds and in the intensity and location of the SPCZ.

3.3. Relationships Between the Wind Stress, SST and SLP Anomalies in the Tropical Pacific

[18] Figure 7a shows the result of the correlation analysis of the QD-scale components of the zonal wind stress anomalies to the south of the equator (10°S–4°S, 180°–120°W) versus the SLP anomalies. This figure suggests that the westerly (easterly) zonal wind stress anomalies to the south of the equator are associated with the positive (negative) SLP anomalies in the western tropical South Pacific and the negative (positive) SLP anomalies in the eastern tropical South Pacific, respectively. This relationship between the SLP and the zonal wind stress anomalies in the tropics is similar to that of the ENSO [e.g., *Wang et al.*, 1999]. This pattern can also be well seen in the snapshot shown in Figure 7, wherein the positive and negative SLP anomalies distribute in the western and eastern tropical Pacific, respectively, and the westerly wind stress anomalies appear to the south of the equator.

[19] It can be seen from Figure 8 that the positive (negative) SST anomalies appear in the eastern tropical Pacific (10°S–10°N, 140°W–100°W) around the Niño-3 region, when the SLP anomalies in the western tropical Pacific is positive (negative). This suggests that the El Niño (La Niña)-like QD-scale SST and SLP anomaly patterns occur at the same time. This relationship between the SST and SLP anomalies can be seen in the snapshot (Figure 8b). We see that the positive SST anomalies in the eastern tropical Pacific accompany the positive SLP anomalies in the western tropical Pacific and the negative SLP anomalies

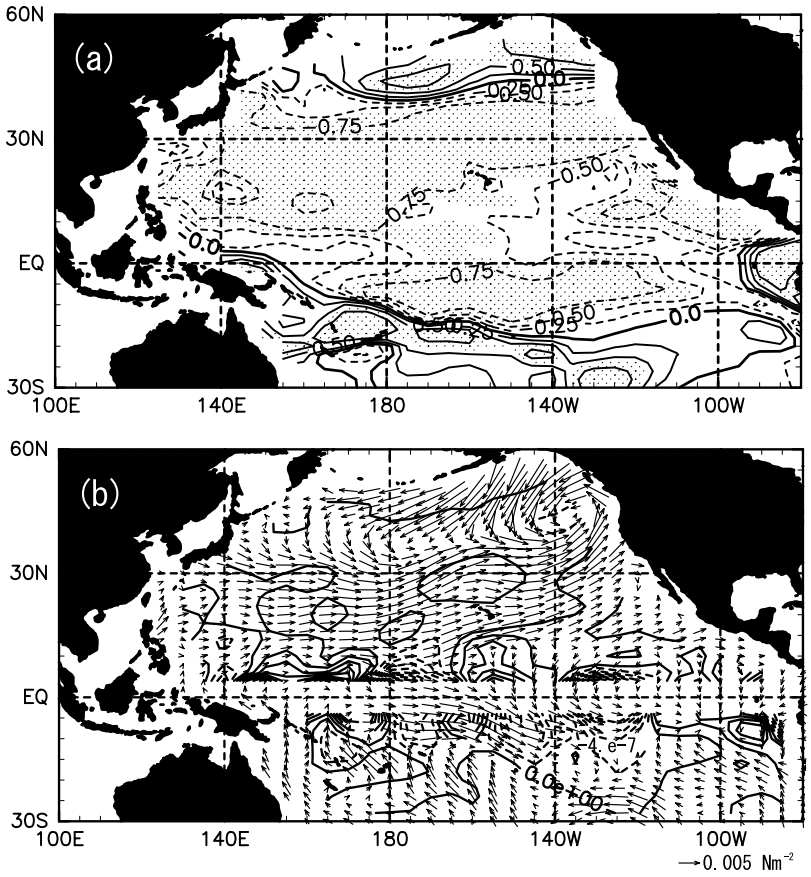

Figure 6. (a) Same as Figure 2 but correlation coefficients between the QD-scale EPV anomalies spatially averaged in the tropical South Pacific (14°S–4°S, 180°–120°W) and the QD-scale zonal wind stress anomalies at each grid point. (b) Snapshot of the QD-scale EPV anomalies and wind stress anomaly vector in the winter of the year 1983. Contour interval of the EPV anomaly is 2.0×10^{-7} m/s, and dashed lines indicate negative anomalies.

in the eastern tropical Pacific. On the basis of Figures 7 and 8, it can be summarized that the El Niño (La Niña)-like QD-scale SST and SLP anomaly patterns accompany the westerly (easterly) wind stress anomalies to the south of the equator. The spatial patterns of the correlation coefficients in Figures 7a and 8a, and snapshots in Figures 7b and 8b are very similar to the ENSO-like, QD-scale wind stress, SLP and SST anomaly patterns found in previous studies [e.g., *Tourre et al.*, 2001]. The new in the present study is that the ENSO-like, QD-scale SST and SLP anomaly patterns are associated with the QD-scale variation of the zonal wind stress to the south of the equator and the Sverdrup transport variations in the tropical South Pacific, which generate the QD-scale *OHC-EP* variations.

[20] The well-known PDO also displays an ENSO-like SST anomaly pattern, and it is dominant on the interdecadal timescale (with a period of about 20 years) and pentadecadal timescale (period of about 50 years) [e.g., *Mantua et al.*, 1997; *Minobe*, 1999]. Here it is worthwhile to compare the PDO and QD-scale SST variations. Figure 9 shows the first EOF (Empirical Orthogonal Function) mode of the QD-scale SST anomalies. This mode can account for approximately 66% of the total variance. The spatial pattern (Figure 9b) is similar to the well-known, ENSO-like, QD-scale SST anomaly pattern, and is consistent to the spatial pattern of the QD-scale SST anomalies (Figure 8b). The PDO index on lower frequency than the interdecadal scale (period longer than 15 years) is also displayed in Figure 9a. We can see that the warm phase of the PDO (the period of the positive PDO index; tropical Pacific SST anomalies take positive values in this period) dominates after the year 1977 and weakens after the mid 1990s as pointed out by previous studies [e.g., *Mantua et al.*, 1997]. On the other hand, warm phase of the QD-scale SST anomaly (positive EOF time coefficients) prevails during the period from the year 1978 to 1985 and from the year 1993 to 1999. During these periods, the positive QD-scale SST anomalies are found in the central and eastern tropical Pacific.

[21] Therefore both the PDO and QD signals have strong positive SST anomalies in the central and eastern equatorial Pacific during the period from the late 1970s to the mid 1980s. However, the cold phase of the QD-scale SST anomaly persists from the year 1986 to 1992, although the PDO is in the warm phase during this period. On the basis of this result, it can be said that the PDO and QD-scale SST anomalies are not always in phase. The differences between the PDO and QD-scale SST anomaly is also observed at midlatitudes. That is, the signals of the QD scale in the midlatitudes are weaker than that of the tropical Pacific (see Figures 8b and 9b), while the PDO has

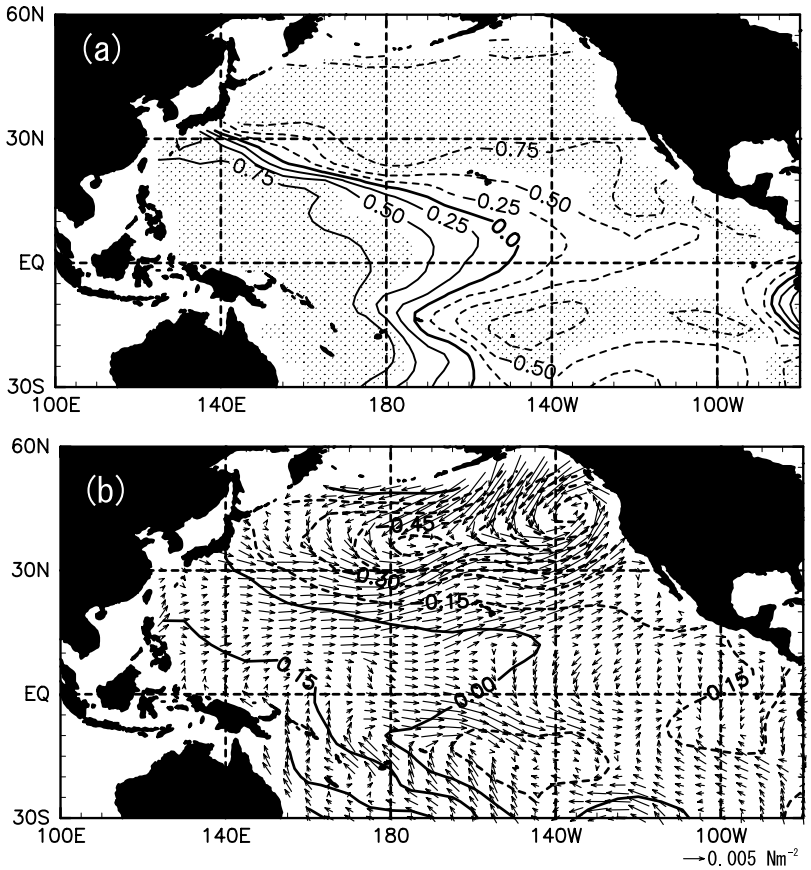

Figure 7. (a) Same as in Figure 2 but the correlation coefficients between the QD-scale zonal wind stress anomalies spatially averaged in the south of the equator (10°S–4°S, 180°–120°W) and the QD-scale SLP anomalies at each grid point. (b) Snapshot of the QD-scale SLP anomalies (contour) and wind stress anomaly vector in the winter of the year 1983. Contour interval of the SLP anomaly is 0.15 hPa, and dashed lines indicate negative anomalies.

stronger signals of SST anomalies at the midlatitudes as compared to the tropical Pacific [e.g., *Mantua et al.*, 1997]. Therefore these results suggest that the QD-scale tropical climate variability is not perfectly explained by the PDO, and its physical mechanism(s) might be different from that of the PDO.

3.4. A Relationship Between the Propagating OHC Anomalies and the *OHC-EP*

[22] Previous studies have pointed out the QD-scale OHC propagations in the tropical North and South Pacific, as was described in the Introduction. Figures 10a through 10c show the time-longitude diagrams of the OHC anomalies along the 14°N–16°N zonal band where the westward propagating QD-scale OHC anomalies are pointed out in previous studies; the 14°S–16°S zonal band where the westward propagations of the QD-scale OHC anomalies are observed; and along the equator (6°S–6°N) where the eastward propagations of the QD-scale OHC anomalies are observed. If the zonal bands are changed from 10°N to 20°N (2°S to 2°N) for the off-equatorial band (for the equatorial band), the main results are unchanged.

[23] We can see that the OHC anomalies propagate westward along the off-equatorial tropical North Pacific (Figure 10a), and after reaching the western boundary, they propagate farther eastward along the equator (Figure 10c). Such counterclockwise propagation characteristics are consistent with those found in previous studies. The eastward propagating OHC anomalies reflect at the eastern boundary and then propagate westward along the off-equatorial Pacific (Figure 10a). The OHC anomalies along the off-equatorial Pacific undergo changes in the phase speed and amplitude to the west of the International Date Line as we will describe in the following (Figure 10a). Along the off-equatorial zonal band, the phase speeds to the east and west of the International Date Line are roughly −0.04 m/s and −0.07 m/s, respectively. Both these phase speeds are slower than that of the theoretical first-mode baroclinic Rossby wave [*Killworth et al.*, 1997]. This result is consistent with the phase speed of the off-equatorial, westward moving signals of the 18°C isotherm depth anomalies in the western off-equatorial Pacific (roughly −0.06 m/s) [*White et al.*, 2003]. The maximum amplitudes of the OHC anomalies near the eastern boundary are greater than 0.1°C, and they then become less than 0.1°C around 160°W. Afterward, they again become greater than 0.1°C to the west of the International Date Line.

[24] This changes in the OHC amplitudes and phase speeds may be due to atmospheric forcing as pointed out by *White et al.* [2003]. In the present study we also

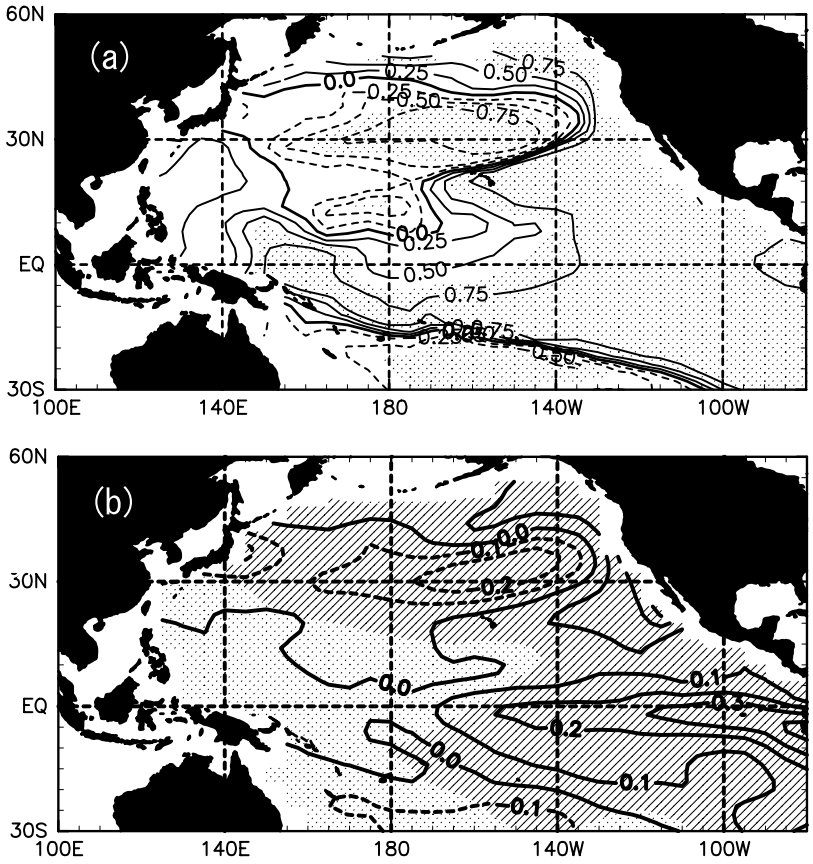

Figure 8. (a) Same as Figure 2 but correlation coefficients between the QD-scale SLP anomalies spatially averaged in the western tropical Pacific (10°S–10°N, 140°E–170°E) and the QD-scale SST anomalies at each grid point. (b) Snapshot of the QD-scale SST anomalies (contour) and the SLP anomalies (shade) in the winter of the year 1983. Contour interval of the SST anomaly is 0.1°C and broken lines indicate negative anomalies. Dotted (slashed) areas mean positive (negative) SLP anomalies.

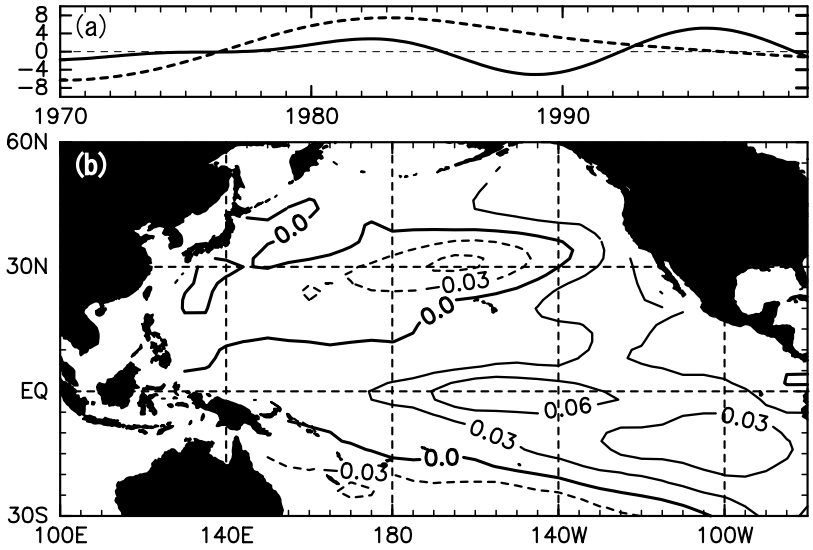

Figure 9. (a) Time coefficients (solid line) and (b) spatial pattern of the first EOF mode for the QD-scale SST anomalies. In Figure 9a, the PDO index with period longer than 15 years is also shown by a dashed line. The values of the PDO index are magnified 10 times their original values for easy viewing.

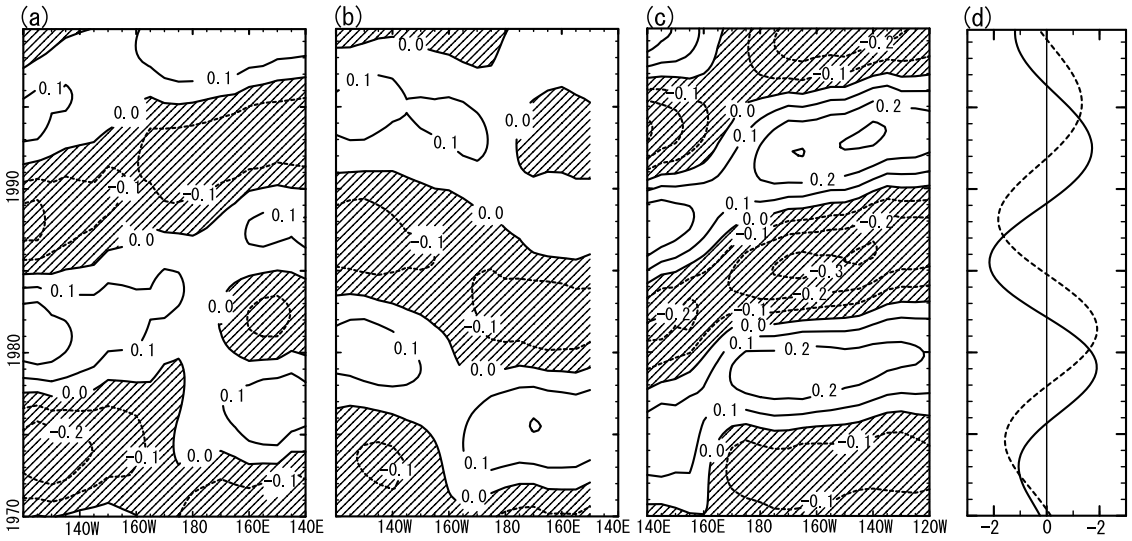

Figure 10. (a) Time-longitude diagram of the QD-scale OHC anomaly along 14°N–16°N. Note that the horizontal axis indicates zonal line from 120°W to 140°E. Negative values are shaded and indicated by broken lines and the contour interval is 0.1°C (b) Same as Figure 10a but along 14°S–16°S. (c) Same as Figure 10a but along 6°S–6°N from 140°E to 120°W. (d) Time series of the normalized *OHC-EP* (thick solid line) and the SST anomalies (thin dashed line) spatially averaged over the eastern tropical Pacific (10°S–10°N, 140°W–100°W) on the QD scale.

investigate the relationship between the westward OHC propagation and the EPV anomalies on the QD scale. Figures 11a through 11c show the time-longitude diagrams of the OHC and EPV anomalies along the 14°N–16°N zonal band, and time series of the SST anomalies averaged over the eastern tropical Pacific, respectively. We can see that after the periods of the positive (negative) peak of the eastern tropical Pacific SST anomalies (Figure 11c), large positive (negative) EPV anomalies appear near the International Date Line from 150°W to 180° (Figure 11b). These positive (negative) EPV anomalies can generate the positive (negative) OHC anomalies by deepening (shallowing) the thermocline. Actually we can see that the westward propagating positive (negative) OHC anomalies are enhanced to the west of the International Date Line, when the positive (negative) EPV anomalies appear (Figures 11a and 11b). It

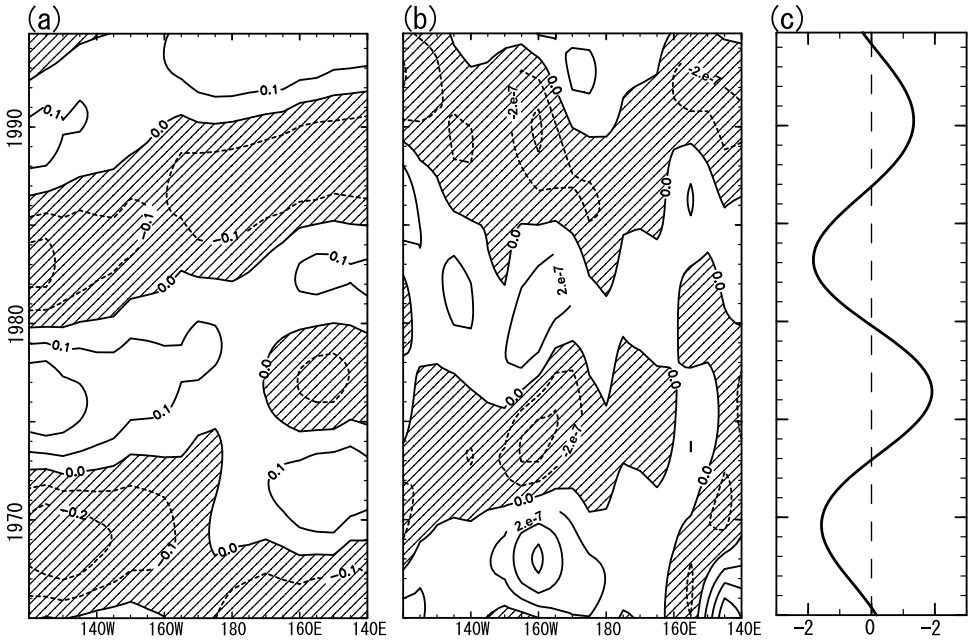

Figure 11. (a) Same as Figure 10a. (b) Same as Figure 10a but the QD-scale EPV anomalies. (c) Time series of the normalized SST anomalies spatially averaged over the eastern tropical Pacific (10°S–10°N, 140°W–100°W) on the QD scale.

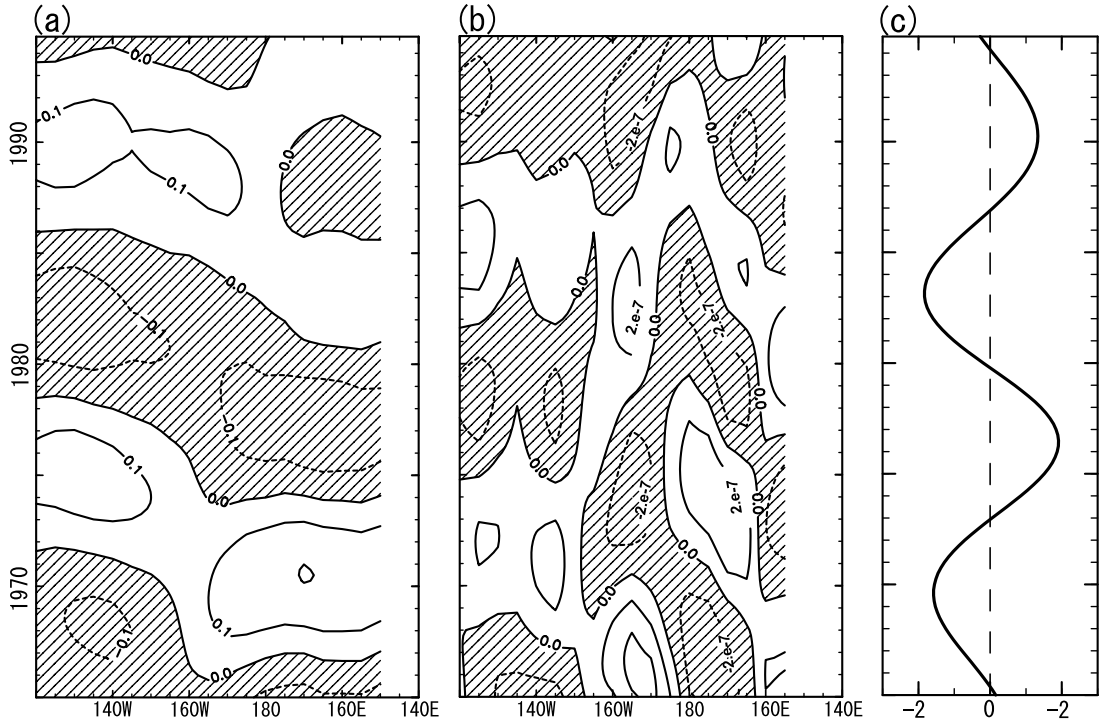

Figure 12. (a) Same as Figure 10b. (b) Same as Figure 10b but the QD-scale EPV anomalies. (c) Same as Figure 11c.

is interesting that the EPV anomalies, i.e., wind stress curl anomalies, in the central basin responds after SST anomalies appear along the equator, having a delay time of several seasons. This delay time is much longer than those for conventional ocean–atmospheric feedbacks in the tropics. Currently we have no idea of a mechanism of the ocean–atmosphere feedbacks on the QD scale. In future, it should be explored by observational, numerical model and theoretical studies.

[25] In the tropical South Pacific, large signals of the OHC anomalies are also observed in the western off-equatorial tropical Pacific, and they connect to the equatorial Pacific as well as the North Pacific (Figure 10b) as pointed by previous studies. However, there is a difference between the North and South Pacific. That is, westward propagations of the OHC anomalies are not seen in the eastern part of the tropical South Pacific, although the equatorial, eastward propagating OHC anomalies reflect at the eastern boundary in the tropical South Pacific as well as in the tropical North Pacific. Therefore it can be said that the reflection of the OHC anomalies at the eastern boundary cannot generate westward propagating OHC anomalies in the eastern part of the tropical South Pacific, in contrast to that in the North Pacific.

[26] We also investigate the relationships between the large OHC anomalies in the western tropical South Pacific and the EPV anomalies. Figures 12a through 12c show a time-longitude diagram of the OHC and EPV anomalies along the 14°S–16°S zonal band, and time series of the SST anomalies averaged over the eastern tropical Pacific, respectively. It can be seen that the large positive (negative) EPV anomalies appear around the International Date Line after the positive (negative) peaks of SST anomalies (Figures 12b and 12c), and then positive (negative) OHC anomalies grow to the west of the International Date Line. This relationship among the OHC, EPV and SST anomalies are similar to those seen in the North Pacific.

[27] Relationship between the propagating OHC anomalies in the off-equatorial tropical North and the South Pacific and the temporal variation of the *OHC-EP* observed in Figures 10a through 10d is as follows. Large positive OHC anomalies are found in the off-equatorial North Pacific along the eastern boundary, having values greater than 0.2°C around the year 1980 (Figure 10a). The positive OHC anomalies propagate westward, and they reach the western boundary in the year 1985 (Figure 10a). In the off-equatorial South Pacific, weak positive OHC anomalies are also found near the western boundary after the year 1986 (Figure 10b). Both positive OHC anomalies in the off-equatorial North and South Pacific reach the western equatorial Pacific (Figures 10a through 10c). Afterward, they start to propagate eastward along the equator from the western equatorial Pacific (Figure 10c). During this time, the *OHC-EP* are increasing in their magnitudes; the normalized *OHC-EP* take large negative values of about −2.0 in the year 1985 and then change to small positive values of about 0.7 around the year 1990 (Figure 10d). The eastward propagating positive OHC anomalies take large values exceeding 0.3°C in the central/eastern equatorial Pacific in the year 1993 (Figure 10c). At the same time, the normalized *OHC-EP* take peak positive values of over 1.8 (Figure 10d). On the other hand, negative OHC anomalies having values of −0.1°C are found in the off-equatorial eastern North Pacific in the year 1987 (Figure 10a). They then propagate westward following the initial positive OHC anomalies, and reach the western boundary after the year 1990 (Figure 10a). At the same time, weak negative OHC anomalies are found in

the off-equatorial western South Pacific (Figure 10b). The both off-equatorial negative OHC anomalies in the North and South Pacific reach the western equatorial region, and then begin to move eastward along the equator after the year 1990 (Figures 10a through 10c). Then the *OHC-EP* are, in turn, decreasing in their magnitudes; values of the normalized *OHC-EP* changes from about 1.8 to −1.1 after the year 1993 (Figure 10d). During this stage, the equatorial propagating positive OHC anomalies get reflected at the eastern boundary (Figure 10c), and then move westward along the off-equatorial band (Figure 10a). This relationship between the equatorial positive (negative) OHC anomalies coming from the off equator and an increase (decrease) of *OHC-EP* in their magnitudes are also found during the period from the year 1970 to 1985.

[28] When the *OHC-EP* take peak positive (negative) values and the off-equatorial propagating negative (positive) OHC anomalies reach the western boundary, the sign of SST anomalies in the eastern tropical Pacific changes from negative (positive) to positive (negative) (Figures 10a and 10d). The result of lag correlation analysis between the *OHC-EP* and the eastern tropical Pacific SST anomalies shows that the SST anomalies in the eastern tropical Pacific lag the *OHC-EP* by 10 seasons (about 3 years) (not shown here). The positive (negative) SST anomalies accompany the El Niño-like (La Niña-like), QD-scale SST and SLP patterns, which cause poleward (equatorward) Sverdrup transport anomalies in the tropical South Pacific as described in previous subsections. At the same time, the negative (positive) OHC anomalies coming from the off-equatorial North and South Pacific enter the equator as shown in Figures 10a and 10b. It can therefore be stated that the negative (positive) propagating OHC anomalies from the off-equatorial North Pacific toward the equator can generate the negative (positive) *OHC-EP* together with the poleward (equatorward) Sverdrup transport in the tropical South Pacific. Although westward propagations of negative (positive) OHC anomalies are not seen in the off-equatorial eastern South Pacific at that time, the negative (positive) OHC anomalies appear at the off-equatorial western South Pacific responding the local negative (positive) EPV anomalies and they then generate the negative (positive) *OHC-EP* together with the negative (positive) OHC anomalies from the North Pacific and the poleward (equatorward) Sverdrup transports in the tropical South Pacific.

4. Summary and Discussion

[29] In this study we investigated the relationships among the equatorial QD-scale OHC anomalies and other related variables in the tropical Pacific by the analysis of oceanic and atmospheric observations. On the basis of the present results, we can summarize the oceanic and atmospheric variations on the QD scale using the schematic picture illustrated in Figure 13. It is assumed that the *OHC-EP* take small positive values initially, and then begin to attain peak positive values. During this time, positive OHC anomalies propagate eastward toward the central/eastern Pacific along the equator, while negative ones propagate westward along the off-equatorial North Pacific after reflection at the eastern boundary (Figure 13a). Thereafter, the signals of the off-equatorial propagating negative OHC anomalies in the North Pacific are enhanced by the local negative EPV anomalies. Negative OHC anomalies are also generated by the local negative EPV anomalies in the off-equatorial tropical South Pacific west of the International Date Line. When the *OHC-EP* take positive peaks, the SST anomalies take weak positive values in the eastern equatorial Pacific. During this stage, the equatorial positive OHC anomalies approach the eastern boundary, and the off-equatorial negative propagating OHC anomalies approach the western boundary, both in the tropical North and South Pacific (Figure 13b).

[30] The positive SST anomalies accompany the El Niño-like, QD-scale SST and SLP anomaly patterns, which trigger westerly zonal wind stress anomalies in the south of the equator accompanied by a cyclonic wind stress anomaly pattern in the tropical South Pacific. Resultantly the cyclonic wind stress anomalies generate negative EPV anomalies centered in the tropical South Pacific. The negative EPV anomalies, in turn, cause a poleward Sverdrup transport in the tropical South Pacific. As a result, the initial positive *OHC-EP* start to decrease in magnitude. The SST and atmospheric anomaly patterns develop well about three years after the positive peak of the *OHC-EP*. At the same time the off-equatorial propagating negative OHC anomalies in the North and South Pacific move toward the equator, and then propagate eastward along the equator after reflecting at the western boundary (Figure 13c). During that time, the positive OHC anomalies in the eastern equatorial Pacific get reflected at the eastern boundary and then start to propagate westward in the off-equatorial North Pacific.

[31] The negative OHC anomalies coming from the off-equator to the equatorial Pacific can also cause a decrease of the *OHC-EP* in their magnitudes. The results can, therefore, be summarized that both the equatorial negative propagating OHC anomalies coming from the off-equatorial North and South Pacific, and the poleward Sverdrup transport in the tropical South Pacific cause a decrease of the *OHC-EP* in their magnitudes. Finally, the initial positive *OHC-EP* change to negative (Figure 13d), and the process continues with the reversal of the sign.

[32] Previous studies have indicated that the off-equatorial North and/or South Pacific play an important role in the generation of the QD-scale thermal anomalies in the equatorial Pacific through wave propagation, gyre circulation change, or Sverdrup transport variations [e.g., *Luo and Yamagata*, 2001; *Jin et al.*, 2001; *McPhaden and Zhang*, 2002; *Nonaka et al.*, 2002; *Hasegawa and Hanawa*, 2003b; *White et al.*, 2003; *Luo et al.*, 2003; *Wang et al.*, 2003]. In the present study, we proposed an additional insight on the linkage between the recharge-discharge oscillator-like, QD-scale variations and the QD-scale OHC propagations in the North and South tropical Pacific. The present results suggest that the QD-scale OHC anomalies in the equatorial Pacific can be generated not only by the Sverdrup transport variation in the tropical South Pacific but also by the ENSO-like, QD-scale propagating OHC anomalies in the tropical North and South Pacific. These combined effects of the propagating OHC anomalies and the Sverdrup transports are very similar with the idea of the unified oscillator model for ENSO dynamics [*Wang*, 2001], which includes various ENSO mechanisms, such as the delayed action oscillator model, the western Pacific oscillator model, the recharge-

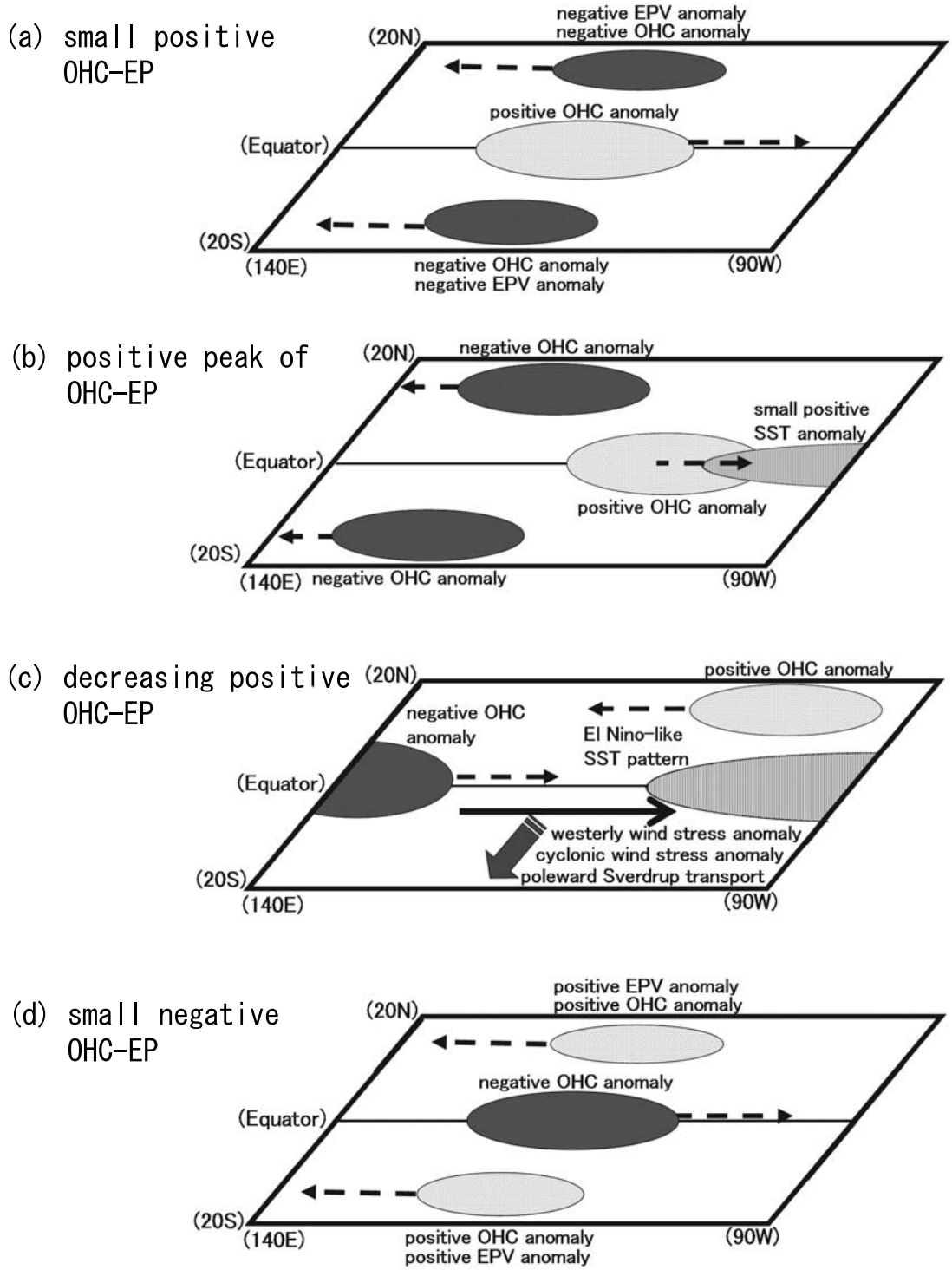

Figure 13. Schematic diagram for a half cycle of the QD-scale oceanic and atmospheric variations in the tropical Pacific.

discharge oscillator model and the advective-reflective oscillator model [*Picaut et al.*, 1997].

[33] Furthermore, the results of this study showed that the QD-scale signal in the tropical Pacific and the PDO are out of phase during a period from the mid 1980s to the mid 1990s. This suggests that the QD-scale signal need its own mechanism different from the PDO. *Tourre et al.* [2001] suggested that the QD-scale variation needs wave propagation in the tropical North and South Pacific, while the interdecadal-scale variation needs advection in the midlatitudes. The present results suggest that the propagating OHC anomalies in the tropical Pacific and also the Sverdrup transport in the tropical South Pacific are responsible for the generation of the QD-scale equatorial OHC anomalies.

Therefore these results contribute to the deeper understanding of the mechanism of the generation of the tropical OHC anomalies on the QD scale.

[34] The present results newly pointed out that the well-known ENSO-like, QD-scale SST and SLP anomaly patterns are associated with the zonal wind stress anomalies and Sverdrup transport variations in the tropical South Pacific, causing the QD-scale equatorial OHC anomalies. The relationship among the QD-scale *OHC-EP*, Sverdrup transport variations and wind stress variations supports the results from numerical model experiments [*Wang et al.*, 2003], but the present results show that such relationship is not dominant in the North Pacific. Further analyses are required to clarify the physical mechanism(s) generating the asymmetry between the North and South Pacific on the QD scale.

[35] **Acknowledgments.** The authors wish to express their sincere thanks to the members of the Oceanographic Research Department at the Meteorological Research Institute and to members of the Physical Oceanography Group at Tohoku University for their useful discussions. The manuscript was also improved through the help of the anonymous reviewers. The first author (Takuya Hasegawa) is supported financially by Research Fellowships of the Japan Society for the Promotion of Science (JSPS) for Young Scientists. The third author (Kimio Hanawa) is supported financially by the Earth Science 21st Century Center-Of-Excellence (COE) program at Tohoku University.

References

Allan, R. J. (2000), ENSO and climatic variability in the last 150 years, in *El Niño and the Southern Oscillation: Multiscale Variability; Global and Regional Impact*, edited by H. F. Diaz and V. Markgraf, pp. 3–55, Cambridge Univ. Press, New York.

Colin, C., C. Henin, P. Hisard, and C. Oudot (1971), Le Courant de Cromwell dans le Pacifique central en février, *Cah. O. R. S. T. O. M. Ser Oceanogr.*, *9*, 167–186.

Deser, C., M. A. Alexander, and M. S. Timlin (1999), Evidence for a wind-driven intensification of the Kuroshio Current extension from the 1970s to the 1980s, *J. Clim.*, *12*, 1696–1706.

Hasegawa, T., and K. Hanawa (2003a), Heat content variability related to ENSO events in the Pacific, *J. Phys. Oceanogr.*, *33*, 407–421.

Hasegawa, T., and K. Hanawa (2003b), Decadal-scale variability of upper ocean heat content in the tropical Pacific, *Geophys. Res. Lett.*, *30*(6), 1272, doi:10.1029/2002GL016843.

Hasegawa, T., and K. Hanawa (2006), Impact of quasi-decadal variability in the tropical Pacific on ENSO modulations, *J. Oceanogr.*, *62*, 227–234.

Hasegawa, T., and K. Hanawa (2007), Upper ocean heat content and atmospheric anomaly fields in the off-equatorial North Pacific related to ENSO, *J. Oceanogr.*, *63*, 561–572.

Hasegawa, T., T. Horii, and K. Hanawa (2006), Two different features of discharge of equatorial upper ocean heat content related to El Niño events, *Geophys. Res. Lett.*, *33*, L02609, doi:10.1029/2005GL024832.

Jin, F.-F. (1996), Tropical ocean-atmosphere interaction, the Pacific cold tongue, and the El Niño–Southern Oscillation, *Science*, *274*, 76–78.

Jin, F.-F. (1997a), An equatorial ocean recharge paradigm for ENSO. Part I: Conceptual model, *J. Atmos. Sci.*, *54*, 811–829.

Jin, F.-F. (1997b), An equatorial ocean recharge paradigm for ENSO. Part II: A stripped-down coupled model, *J. Atmos. Sci.*, *54*, 830–847.

Jin, F.-F., M. Kimoto, and X. Wang (2001), A model of decadal ocean-atmosphere interaction in the North Pacific basin, *Geophys. Res. Lett.*, *28*, 1531–1534.

Kalnay, E., et al. (1996), The NCEP/NCAR 40-year reanalysis project, *Bull. Am. Meteorol. Soc.*, *77*, 437–471.

Kessler, W. S. (1990), Observations of long Rossby waves in the northern tropical Pacific, *J. Geophys. Res.*, *95*, 5183–5217.

Kessler, W. S. (2002), Is ENSO a cycle or a series of events?, *Geophys. Res. Lett.*, *29*(23), 2125, doi:10.1029/2002GL015924.

Killworth, P. D., D. B. Chelton, and R. A. deZoeke (1997), The speed of observed and theoretical long extra-tropical planetary waves, *J. Phys. Oceanogr.*, *27*, 1946–1966.

Knutson, T. R., and S. Manabe (1998), Model assessment of decadal variability and trends in the tropical Pacific ocean, *J. Clim.*, *11*, 2272–2296.

Ladd, C., and L. A. Thompson (2000), Formation mechanisms for North Pacific central and eastern subtropical mode waters, *J. Phys. Oceanogr.*, *30*, 868–887.

Luo, J., and T. Yamagata (2001), Long-term El Niño-Southern Oscillation (ENSO)-like variation with special emphasis on the South Pacific, *J. Geophys. Res.*, *106*, 22,211–22,227.

Luo, J., S. Masson, S. Behera, P. Delecluse, S. Gualdi, A. Navarra, and T. Yamagata (2003), South Pacific origin of the decadal ENSO-like variation as simulated by a coupled GCM, *Geophys. Res. Lett.*, *30*(24), 2250, doi:10.1029/2003GL018649.

Mann, M. E., and J. Park (1996), Joint spatiotemporal modes of surface temperature and see level pressure variability in the northern hemisphere during the last century, *J. Clim.*, *9*, 2137–2162.

Mantua, N. J., S. R. Hare, Y. Zhang, J. M. Wallace, and R. C. Francis (1997), A Pacific interdecadal climate oscillation with impacts on salmon production, *Bull. Am. Meteorol. Soc.*, *78*, 1069–1079.

McPhaden, M. J., and D. Zhang (2002), Slowdown of the meridional overturning circulation in the upper Pacific Ocean, *Nature*, *415*, 603–608.

Meinen, C. S., and M. J. McPhaden (2000), Observations of warm water volume changes in the equatorial Pacific and their relationship to El Niño and La Niña, *J. Clim.*, *13*, 3551–3559.

Minobe, S. (1997), A 50–70 year climatic oscillation over the North Pacific and the North America, *Geophys. Res. Lett.*, *24*, 683–684.

Minobe, S. (1999), Resonance in bidecadal and pentadecadal climate oscillations over the North Pacific: Role in climate regime shifts, *Geophys. Res. Lett.*, *26*, 855–858.

Nitta, T., and S. Yamada (1989), Recent warming of tropical sea surface temperature and its relationship to the Northern Hemisphere circulation, *J. Meteorol. Soc. Jpn.*, *67*, 375–383.

Nonaka, M., S.-P. Xie, and J. P. McCreary (2002), Decadal variations in the subtropical cells and equatorial pacific SST, *Geophys. Res. Lett.*, *29*(7), 1116, doi:10.1029/2001GL013717.

Picaut, J., F. Masia, and Y. du Penhoat (1997), An advective-reflective conceptual model for the oscillatory nature of the ENSO, *Science*, *277*, 663–666.

Smith, T. M., and R. W. Reynolds (2003), Extended reconstruction of global sea surface temperatures based on COADS data (1854–1997), *J. Clim.*, *16*, 1495–1510.

Suarez, M. J., and P. S. Schopf (1998), A delayed action oscillator for ENSO, *J. Atmos. Sci.*, *45*, 3283–3287.

Tanimoto, Y., N. Iwasaka, K. Hanawa, and Y. Toba (1993), Characteristic variations of sea surface temperature with multiple time scales in the North Pacific, *J. Clim.*, *6*, 1153–1160.

Tanimoto, Y., N. Iwasaka, and K. Hanawa (1997), Relationship between sea surface temperature, the atmospheric circulation and air-sea fluxes on multiple time scales, *J. Meteorol. Soc. Jpn.*, *75*, 831–849.

Torrence, C., and G. P. Compo (1998), A practical guide to wavelet analysis, *Bull. Am. Meteorol. Soc.*, *79*, 61–78.

Tourre, Y. M., B. Rajagopalan, Y. Kushnir, M. Barlow, and W. B. White (2001), Patterns of coherent decadal and interdecadal climate signals in the Pacific Basin during the 20th century, *Geophys. Res. Lett.*, *28*, 2069–2072.

Tourre, Y. M., C. Cibot, L. Terray, W. B. White, and B. Dewitte (2005), Quasi-decadal and inter-decadal climate fluctuations in the Pacific Ocean from a GCM, *Geophys. Res. Lett.*, *32*, L07710, doi:10.1029/2004GL022087.

Trenberth, K. E. (1990), Recent observed interdecadal climate changes in the Northern Hemisphere, *Bull. Am. Meteorol. Soc.*, *71*, 988–993.

Wang, C. (2001), A unified oscillator model for the El Niño–Southern Oscillation, *J. Clim.*, *14*, 98–115.

Wang, C., R. H. Weisberg, and J. I. Virmani (1999), Western Pacific interannual variability associated with the El Niño-Southern Oscillation, *J. Geophys. Res.*, *104*, 5131–5149.

Wang, X., F.-F. Jin, and Y. Wang (2003), A tropical ocean recharge mechanism for climate variability. Part II: A unified theory for decadal and ENSO modes, *J. Clim.*, *16*, 3599–3616.

Weisberg, R. H., and C. Wang (1997), A western oscillator paradigm for the El Niño-Southern Oscillation, *Geophys. Res. Oceanogr.*, *6*, 671–678.

White, W. B. (1995), Design of a global observing system for gyre-scale upper ocean temperature variability, *Prog. Oceanogr.*, *36*, 169–217.

White, W. B., and D. R. Cayan (1998), Quasi-periodicity and global symmetries in interdecadal upper ocean temperature variability, *J. Geophys. Res.*, *103*, 21,335–21,354.

White, W. B., and D. R. Cayan (2000), A global El Niño–Southern Oscillation wave in surface temperature and pressure and its interdecadal modulation from 1900 to 1997, *J. Geophys. Res.*, *105*, 11,223–11,242.

White, W. B., Y. M. Tourre, M. Barlow, and M. Dettinger (2003), A delayed action oscillator shared by biennial, interannual, and decadal signals in the Pacific Basin, *J. Geophys. Res.*, *108*(C3), 3070, doi:10.1029/2002JC001490.

Yasunaka, S., and K. Hanawa (2002), Regime shifts found in the Northern Hemisphere SST field, *J. Meteorol. Soc. Jpn.*, *80*, 119–135.

Yasunaka, S., and K. Hanawa (2003), Regime shifts in the Northern Hemisphere SST field: Revisited in relation to tropical variations, *J. Meteorol. Soc. Jpn.*, *81*, 415–424.

Yasunaka, S., and K. Hanawa (2005), Regime shifts and ENSO events in the global SSTs, *Int. J. Climatol.*, *25*, 913–930, doi:10.1002/joc.1172.

Yukimoto, S., M. Endoh, Y. Kitamura, A. Kitoh, T. Motoi, and A. Noda (2000), ENSO-like interdecadal variability in the Pacific Ocean as simulated in a coupled general circulation model, *J. Geophys. Res.*, *105*, 13,945–13,963.

Zhang, R. H., and S. Levitus (1996), Structure and evolution of interannual variability of the tropical Pacific upper ocean temperature, *J. Geophys. Res.*, *101*, 20,501–20,524.

Zhang, T. Y., J. M. Wallace, and D. S. Battisti (1997), ENSO-like interdecadal variability: 1900–93, *J. Clim.*, *10*, 1004–1020.

K. Hanawa, Physical Oceanography Laboratory, Department of Geophysics, Graduate School of Science, Tohoku University, 6-3 Aramaki-aza-Aoba, Aoba-ku, Sendai 980-8578, Japan. (hanawa@pol.geophys.tohoku.ac.jp)

T. Hasegawa, Institute of Observation Research for Global Change, Japan Agency for Marine-Earth Science and Technology, 2-15 Natsushima-Cho, Yokosuka 237-0061, Japan. (takuyah@jamstec.go.jp)

T. Yasuda, Climate Research Department, the Meteorological Institute, the Japan Meteorological Agency, 1-1 Nagamine, Tsukuba, Ibaraki 305-0052, Japan. (tyasuda@mri-jma.go.jp)